ACS OMEGA

http://pubs.acs.org/journal/acsodf

Article

Color Space Transformation-Based Algorithm for Evaluation of Thermochromic Behavior of Cholesteric Liquid Crystals Using Polarized Light Microscopy

Shani L. Levit,[§] Jimmy Nguyen,[§] Nicholas P. Hattrup, Briget E. Rabatin, Ratib Stwodah, Christopher L. Vasey, Michael P. Zeevi, McKenna Gillard, Paola A. D'Angelo, Kathleen W. Swana, and Christina Tang*

Cite This: *ACS Omega* 2020, 5, 7149−7157

Read Online

ACCESS | Metrics & More | Article Recommendations | Supporting Information

ABSTRACT: Cholesteryl ester liquid crystals exhibit thermochromic properties related to the existence of a twisted nematic phase. When used in applications such as thermal mapping, a color change is often monitored by video cameras. Thus, quantitative methods to evaluate thermochromic behavior (e.g., blue-start, red-start, red-end, color play and bandwidth) from video analysis are desirable. However, obtaining quantitative color measurements from digital images remains a significant technical challenge, especially for highly reflective samples such as liquid crystals (for which ultraviolet−visible (UV−vis) reflectance spectroscopy is typically used). We developed a method to determine thermochromic properties from videos of liquid crystal cooling under polarized light microscopy. We relate observed color transitions to quantifiable changes in the cumulative color difference in the International Commission on Illumination (CIE) $L^*a^*b^*$ color space and validate this method with UV−vis reflectance spectroscopy. The measured thermochromic behavior and associated measurement uncertainties (coefficient of variations) were comparable to UV−vis reflectance measurements.

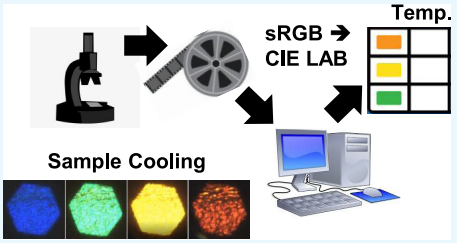

INTRODUCTION

Cholesterol ester liquid crystals demonstrate thermochromic behavior, which results from the temperature-dependent pitch length of a twisted nematic phase.[1,2] A decrease in temperature causes untwisting of the helical structure leading to an increase in the pitch length.[1,2] At high temperatures (i.e., above the mesophases transition temperature), the isotropic liquid appears clear.[1,2] Upon cooling, the liquid crystal phase reflects visible light.[1,2] As the temperature decreases, the liquid crystal first reflects blue light, λ = 450 nm, at relatively short pitch lengths.[1,2] With further decreases in temperature, the wavelength reflected shifts to the red-end of the spectrum (λ = 760 nm) due to the increase in the pitch length.[1,2] Eventually, the liquid crystal phase appears opaque as the resulting increase in the pitch reflects light outside the visible wavelength range. Such materials have been used in thermal mapping and analysis in medical, industrial, and engineering applications.[3−9]

Since the thermochromic properties of liquid crystals are related to the mesophase transition, characterization of their thermal properties via differential scanning calorimetry (DSC) has been widely studied and reported.[10−12] The change in the pitch and resulting color transition as a function of temperature is nonlinear and occurs above the measured Smectic A to twisted nematic (S_A*−N*) transition temperature and the enthalpy of the S_A*−N* transition affects the rate of color change upon cooling.[2] However, the temperature-dependent color liquid crystal formulations are not fully described by their thermal properties.

Practically, the thermochromic behavior of liquid crystals can be described with various metrics.[1] The start temperatures for when blue, green, and red light is first observed are characterized as the blue-start, green-start, and red-start, respectively, as the sample is heated or cooled. The color play region is defined as the entire temperature range across which color is visible and the bandwidth is the temperature range between the blue-start and red-start temperatures. Such metrics of liquid crystals have typically been characterized by ultraviolet−visible (UV−vis) spectroscopy.[1] Given the increased availability of smartphone cameras, leveraging such technology as nontraditional colorimeters is of growing interest.[13] When liquid crystals are applied in thermal mapping, a color change is often monitored by video cameras.[14,15] Thus, quantitative methods to evaluate thermochromic behavior from videos would be valuable.

Received: October 18, 2019
Accepted: March 13, 2020
Published: March 24, 2020

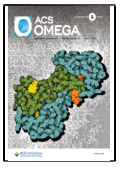

https://dx.doi.org/10.1021/acsomega.9b03484
ACS Omega 2020, 5, 7149−7157

Obtaining quantitative color measurements results from digital images remains a significant technical challenge because the reflectance spectra cannot be calculated from red−green−blue (RGB) values[16] without modeling or estimating the spectral reflectance function of the recording device.[17,18] Previous reports have considered color calibration of RGB digital cameras using commercially available color charts (e.g., GretagMacBeth ColorChecker).[19] However, the color charts are typically of diffusive rather than reflective color samples; color charts viewed with polarizers are not readily available. Additionally, the calibration is device- and setup-dependent.[20] Reflectance spectra can also be estimated from camera measurements using various methods, e.g., regression estimation or machine learning, but are computationally or data intensive.[13,17,18,21,22]

Recently, colorimetry using smartphones has been reported by converting the images from RGB to alternative color spaces such as hue, saturation, and value (HSV) or International Commission on llumination (CIE) $L^*a^*b^*$. The CIE $L^*a^*b^*$ space was defined by the International Commission on Illumination, which is abbreviated CIE. It uses three values to define color, lightness (L), a^* to indicate a red/green value, and b^* to indicate a blue/yellow value.[23,24] Image analyses in the alternate color spaces have been used for various applications including urinalysis,[25] paper-based tests for measuring alcohol concentration in saliva,[26] water quality monitoring,[13] and enzyme-linked immunosorbent assays.[27]

The use of CIE $L^*a^*b^*$ color space has been especially useful for reflective samples.[28] Analysis of changes of $L^*a^*b^*$ values has proven to be an effective means to detect color change using a digital camera.[14,29] Specifically, Panak et al. characterized thermochromic behavior of a leuco dye (i.e., a single color change) by tracking cumulative changes in $L^*a^*b^*$ values as a function of temperature employing a digital camera.[14]

In this work, we aim to develop a method to quantify the thermochromic properties of liquid crystals observed under polarized light microscopy (PLM). This system is challenging to analyze because in addition to changes in sample color, there are changes in sample brightness. Specifically, the samples become brighter in the blue region and fade in the red region. To accurately capture the observed color change, videos were recorded with autoexposure and auto white balance (Supporting Information, Figure S1). Such camera settings are similar to point of care, smartphone technology in which changing environments and image quality are significant concerns.[30] New methods to perform quantitative analysis based on such videos are needed.[30]

To analyze the videos, we transform the sRGB video data to CIE $L^*a^*b^*$ color space and establish an empirical threshold value in a cumulative color change to identify color change events. Subsequently, we distinguish between changes in sample brightness and sample color transitions. Due to the automatic camera settings and the novelty of the analysis method, the focus of our work is validating the video analysis method with UV−vis reflectance spectroscopy to verify that the color transitions identified in the video correspond to the expected changes in UV−vis peak reflectance.

RESULTS AND DISCUSSION

Thermochromic behavior is intrinsic to a liquid crystal molecule arising from its inherent ability to form a twisted nematic phase. The resulting temperature-dependent color is affected by the limiting pitch of the twisted nematic phase (i.e., the pitch without any unwinding) and by the thermodynamic properties such as the mesophase S_A*−N* transition temperature and enthalpy of the mesophase transition. Since individual cholesterol derivative molecules have a limited temperature range for thermochromic behavior, mixtures of cholesterol esters are often formulated to tune the temperature-dependent optical properties.

For example, cholesterol benzoate exhibits a cholesteric mesophase. Both cholesteryl pelargonate (CP) and cholesteryl olyeyl carbonate exhibit a smectic to twisted nematic transitions. Thus, to achieve formulations with thermochromic behavior, we used ternary mixtures of cholesteryl benzoate (CB), cholesteryl pelargonate (CP), and cholesteryl oleyl carbonate (COC). Physically, thermochromic behavior occurs due to Smectic A to the twisted nematic phase transition. Specifically, the thermochromic behavior, i.e., the color transition from blue to red, is observed at temperatures above the Smectic A to twisted nematic (S_A*−N*) phase transition temperature.[2] Since the phase transition is the physical basis for the thermochromic behavior, we began by measuring the effect of composition on this mesophase transition temperature by differential scanning calorimetry (DSC), a practical tool for observing such phase transitions under precise thermal control.[31]

The formulations and the mesophase transition temperatures measured by DSC are shown in Table 1. The ternary mixtures show a mesophase transition temperature between 23.7 ± 0.4 and 36.1 ± 0.2 °C. As expected, combining two mesomorphic compounds (CP and COC) significantly depressed the mesophase transition temperature compared to cholesterol benzoate (previously reported to be 145 °C[32]). Additionally, the mesophase transition temperature was inversely proportional to the fraction of COC in the formulation. LC-1 with the highest COC fraction had the lowest mesophase transition temperature. This result agrees well with previous reports in which COC is used as a low-melting base compound to depress the transition temperature.[33] Therefore, decreasing the fraction of COC in the formulation was expected to increase the transition temperature.

Table 1. Compositions of Liquid Crystal Formulations and Their Mesophase Transition Temperature Measured by Differential Scanning Calorimetry (DSC)

sample	COC (wt %)	CP (wt %)	CB (wt %)	mesophase transition temperature from DSC (°C)
LC-1	60	30	10	23.7 ± 0.4
LC-2	45	45	10	26.6 ± 0.2
LC-3	30	60	10	36.1 ± 0.2

While the Smectic A to twisted nematic phase transition (measured by DSC under precise thermal control) gives rise to the thermochromic behavior, we were interested in directly observing the temperature-dependent color under accessible thermal conditions using polarized light microscopy (PLM). Polarized light microscopy (PLM) is useful for analyzing anisotropic materials such as liquid crystals in the twisted nematic phase. On the PLM, we cooled the liquid crystal from an isotropic liquid at ∼45 °C to ambient conditions, we observed a distinct change from black (isotropic liquid in the PLM) to a bright blue, followed by a transition to green,

https://dx.doi.org/10.1021/acsomega.9b03484
ACS Omega 2020, 5, 7149−7157

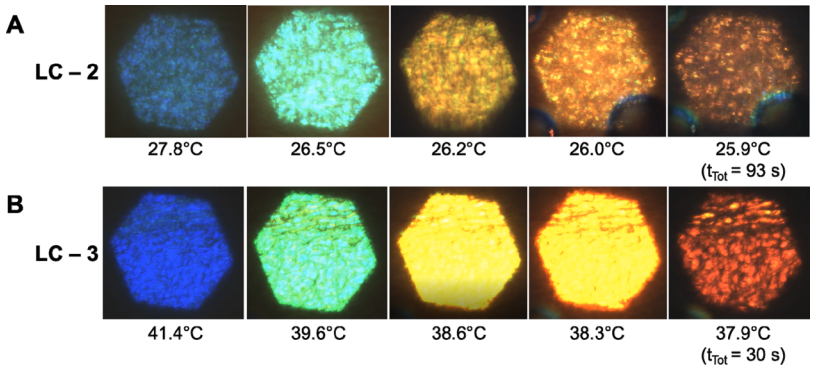

Figure 1. Polarized light microscopy images during LC cooling for (A) LC-2: 45% COC, 45% CP, 10% CB and (B) LC-3: 30% COC, 60% CP, 10% CB. Both samples transition from blue to red while cooling over 1−2 min. The full-color transition (red-end) of LC-1 was not accessible at ambient conditions.

yellow, orange, and then red due to changes in the pitch length as a function of temperature. The red eventually faded to black again for LC-2 and LC-3 (Figure 1). We note that in addition to changes in color, the sample also changes in brightness. Specifically, the samples brightened in the blue region and faded in the red region. Due to this initial sample brightening in the blue region, videos were recorded with autoexposure and auto white balance to capture the perceived color change, i.e., transition from blue to green to yellow to orange to red (examples with and without autoexposure and auto white balance are provided in the Supporting Information, Figure S1). Auto white balance is commonly used to achieve color constancy between images.[34] Such white balance correction algorithms have been used to standardize measurements between environments in smartphone video-based colorimetric methods.[30] In this setup using white balancing with the colorimetrically stable black aperture diaphragm surrounding the thermochromic liquid crystal, the perceived colors of the liquid crystals in the images matched the expected maximum UV−vis reflectance at the corresponding temperature (Figure S2) based on ISO standard 21348. However, we emphasize that the focus of this work is identifying color changes rather than "ground truth colors" to characterize the thermochromic properties of liquid crystals, i.e., the temperature of the color change events.

The thermochromic properties of the two liquid crystal formulations could be estimated from the video analysis by manually performing frame-by-frame analysis to determine the transitions from (1) black to blue, (2) blue to green, (3) green to yellow, (4) yellow to orange, (5) orange to red, and (6) red to black but were observer-dependent. Thus, we aimed to automate analysis of the video to quantify the thermochromic behavior of the liquid crystal formulations via various metrics (blue-start temperature, green-start temperature, red-start temperature, red-end temperature, color play, and bandwidth). We note, for LC-1, the mesophase transition temperature was below ambient temperature. Therefore, the entire thermochromic behavior could not be accessed. Specifically, the red-end temperature and color play could not be determined.

For automated quantitative analysis as an alternative to manual frame-by-frame analysis, we transformed the RGB values extracted from individual frames from the video to CIE $L^*a^*b^*$ color space defining the color of the frame in three values: L indicating brightness, a^* indicating a value for red/green, and b^* indicating a value of blue/yellow. The L^*a^*b space was selected because it correlates strongly with human vision.[23,24] Our aim was to relate the visual color changes with quantitative changes in $L^*a^*b^*$ values.

Specifically, we performed frame-by-frame analysis using the cumulative color difference (color distance, which has been a useful measure for identifying color differences between samples observed between cross polarizers[35]) from the initial frame (black). To identify color change events, we calculated the change in the relative color difference between each frame and the previous frame. Further detail is provided in the Methods section below.

A color change event was said to occur if the change in the relative color difference between consecutive frames was greater than a threshold value of 2.5. This empirically determined threshold is similar to the empirical benchmark previously reported as the "just noticeable" color differences for CIELAB".[36] Generally, this method identified more than six color change events because the sample changed in brightness while changing in color. Specifically, the samples brightened in the blue region and faded in the red region.

Thus, we identified the changes in sample brightness as well as the observed sample color transitions from (1) black to blue, (2) blue to green, (3) green to yellow, (4) yellow to orange, (5) orange to red, and (6) red to black. Based on the physical observations, the first and last identified color changes correspond to the blue-start (black to blue) and red-end (red to black).

Next, we aimed to distinguish between changes in sample brightness and changes in sample color between consecutive frames for the intermediate color changes, i.e., (2) blue to green, (3) green to yellow, (4) yellow to orange, and (5) orange to red. Thus, we examined the fraction of the total frame-to-frame color difference that was due to the difference in L values corresponding to a change in sample brightness, which we defined as $f_{\Delta L}$ (see the Methods section and eq 3 below for more detail). The consecutive frames with the four lowest $f_{\Delta L}$ values were determined to be the color transitions. Typically, $f_{\Delta L}$ values for color transitions were less than 0.02 compared to changes in sample brightness with $f_{\Delta L} > 0.2$. The first color transition after the identified blue-start was considered the blue to green transition. The next identified color transitions were considered the green to yellow, yellow to orange, and orange to red transitions. The identified color transitions using this method were similar to the manual frame-by-frame analysis as initial verification of our approach.

In the previous literature, Panak et al. used color difference, cumulative changes in $L^*a^*b^*$ values as a function of

https://dx.doi.org/10.1021/acsomega.9b03484
ACS Omega 2020, 5, 7149−7157

temperature, to characterize the thermochromic behavior of a leuco dye employing a digital camera calibrated with an X-Rite ColorChecker.[14] Since using constant aperture values was not possible for our system due to the constantly changing sample brightness that occurred simultaneously with the color transition (Figure S1). Our next goal was to validate the color changes identified by the video analysis method with UV−vis reflectance spectroscopy, which is a well-established method for monitoring the color of reflective materials.[37−40] Specifically, we aimed to verify that the color change events that we identified in the video analysis corresponded with changes in the UV−vis reflectance peak.

As the sample cooled, the peak reflectance shifted from 450 nm (blue range) to 610 nm (red). Representative UV−vis reflectance spectra as a function of time after the blue-start are shown in Figure 2. Using UV−vis reflectance measurements, we confirmed that the red-end of LC-1 was not accessible at ambient conditions because of the mesophases transition temperature below ambient temperature. This result agrees with our PLM analysis.

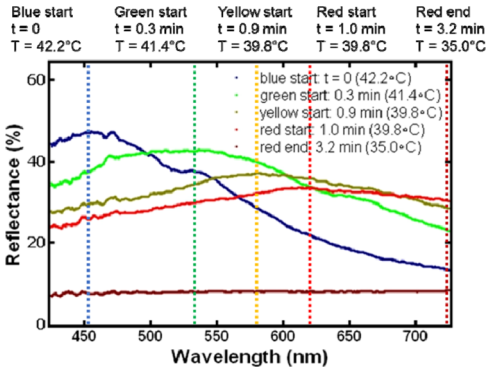

Figure 2. Representative UV−vis reflectance spectra for LC-3 recorded as the sample cooled over several minutes. The peaks in reflectance occurring at 456 nm (blue-start), 537 nm (green-start), 582 nm (yellow-start), 613 nm (red-start), and 723 nm (red-end) correspond to the perceived color. As the sample cooled, the reflectance peak shifted to higher wavelengths due to the transition from blue to red. There is also a decrease in reflectance due to the sample fading.

We also note that the intensity of the reflected color decreases as the sample transitioned to red, similar to our visual observations under PLM. Interestingly, determining all of the individual color start temperatures, e.g., orange-start temperatures from the UV−vis reflectance measurements, was not consistently possible because they were so close together in temperature. In Figure 2, for example, the yellow-start, orange-start, and red-start occur at the same temperature. While increasing the frequency of the scans is possible, increasing the precision of the temperature monitoring would also be required. This challenge arises due to the nonlinear relationship between the pitch and temperature that narrows as the sample approaches the red region.[1,2]

Next, the blue-start, red-start, and red-end temperatures (Table 2) were identified. Comparing the blue-start, red-start, and red-end temperatures determined using UV−vis reflectance spectroscopy to video analysis of PLM, all temperatures are comparable, i.e., less than an 8.5% difference (Table 2). This difference in temperature is comparable to the measurement uncertainty as the coefficient of variation of all of the color transition temperatures was 8.6% or less (Table 2). We also note that since the transition to red occurred at or below ambient conditions for LC-1, the red-start and red-end could not be fully identified using UV−vis reflectance. This result was similar to the PLM result in which the red-end could not be identified from the video analysis. These results indicated that the color change events captured by the video and subsequent analysis correspond to the expected changes in UV−vis peak reflectance (colors corresponding to the reflectance spectra defined using ISO 21348), which validates our approach identifying color change events based on the cumulative color difference in CIE $L^*a^*b^*$ color space.

Interestingly, the start of the color transition (i.e., the blue-start temperature) for the three formulations was evaluated using both PLM and UV reflectance slightly above the mesophase transition temperature measured by DSC (Table 1). This trend is expected as the color transition is expected to occur above the mesophase transition temperature measured by DSC.[2] Since the focus of this work was developing a video analysis method complementary to UV−vis reflectance, further evaluation of LC formulations (especially the red-end temperature) during both heating and cooling at various rates to further investigate their thermochromic behavior will be pursued in future work as both cooling rate[31] and hysteresis[41,42] are known to affect thermochromic behavior.

Based on the measured color transition temperatures, we compared the bandwidth (temperature difference between blue-start and red-start) for LC-2 and LC-3 measured by UV−vis and PLM (Supporting Information, Table S1). Since the transition to red occurred at or below ambient conditions for LC-1, the red-start and red-end could not be fully identified using UV−vis reflectance. This result was similar to the PLM result in which the red-end could not be identified from the video analysis. Our focus is comparing the results for the two different analysis methods rather than understanding the effect of formulation on thermochromic behavior (which has been reported elsewhere[1]). Interestingly, the bandwidth measured by PLM is approximately 2-fold larger than the UV−vis measurements. We note that there may be slight discrepancies when identifying the red-start, a more subtle orange to red

Table 2. Color Transitions Determined by PLM Video Analysis Compared to UV−vis Reflectance Spectroscopy Performed under Similar Thermal Conditions[a]

formulation	UV blue-start (°C)	UV red-start (°C)	UV red-end (°C)	PLM blue-start (°C)	PLM red-start (°C)	PLM red-end (°C)
LC-1	26.3 ± 0.7	<23.6 ± 0.2	<23.2 ± 0.2	25.4 ± 0.6	23.6 ± 0.2	<22.9 ± 0.2
LC-2	30.0 ± 1.3	27.5 ± 1.4	25.5 ± 1.7	30.3 ± 2.6	26.4 ± 0.7	25.3 ± 0.2
LC- 3	40.1 ± 1.8	37.8 ± 1.4	34.0 ± 1.3	42.6 ± 1.8	38.1 ± 2.1	36.9 ± 1.7

[a]The averages and standard deviations from three trials are reported. Overall, the color transition temperatures identified using PLM and UV−vis reflectance are comparable; thus the color change events identified by video analysis correspond with changes in UV−vis peak reflectance validating our approach.

https://dx.doi.org/10.1021/acsomega.9b03484
ACS Omega 2020, 5, 7149−7157

color change than red to black, which could lead to differences in the measured bandwidth. However, given the large coefficient of variation using both techniques, the difference is not statistically significant (student t-test, $\alpha = 0.05$). The color play (temperature difference between blue-start and red-end) measured by PLM is comparable with the UV−vis reflectance spectroscopy (less than 10% difference) (Supporting Information, Table S1). These results suggest that the PLM video analysis method is a complementary approach to UV−vis reflectance for determining the thermochromic properties of liquid crystal formulations. Additionally, this method may be adapted for analyzing thermochromic surfaces commonly used, e.g., thermography.[20,43−51]

Overall, we develop a simple and efficient video analysis method to identify color change events based on the cumulative color difference in CIE $L^*a^*b^*$ color space and subsequently distinguishing between changes in sample brightness and changes in color to determine the thermochromic properties of liquid crystals. Importantly, the color transitions determined from the video analysis correspond to changes in the UV−vis peak reflectance validating our approach. The thermochromic properties and the associated uncertainties (coefficients of variation of color transition temperatures, bandwidth, and color play) determined from the PLM video analysis agree well with the UV−vis reflectance measurements, suggesting that the PLM video analysis method is a complementary approach to UV−vis reflectance for determining the thermochromic properties of liquid crystal formulations.

CONCLUSIONS

We have developed a method to analyze the sRGB video of liquid crystal formulations observed under polarized light microscopy to quantify the thermochromic properties of the liquid crystals. The sRGB data from the video frames are transformed into CIE $L^*a^*b^*$ color space. In CIE $L^*a^*b^*$ color space, we relate observed color transitions, namely, black to blue, blue to green, green to yellow, yellow to orange, orange to red, and red to black, to quantifiable changes in cumulative color difference and distinguish between changes in sample brightness and color transitions. Our approach was validated with UV−vis reflectance spectroscopy; the identified color transitions corresponded with the expected changes in UV−vis peak reflectance. Further, the measured thermochromic properties (bandwidth and color play) were comparable to UV−vis reflectance spectroscopy. Notably, this approach for automatically identifying color change using videos with a fixed black background may be applied to smartphone technology with embedded autoexposure and auto white balance correction algorithms with a wide range of applications.

METHODS

Materials. Liquid crystal components: cholesteryl oleyl carbonate, cholesteryl benzoate, and cholesteryl pelargonate were obtained from Sigma (St. Louis, MO). All chemicals were used as received.

Liquid Crystal Formulation. To achieve thermochromic properties, we formulated ternary mixtures of cholesteryl benzoate (CB), cholesteryl pelargonate (CP), and cholesteryl oleyl carbonate (COC). The ternary mixtures were combined into homogenous solutions by combining appropriate masses of the three components (Table 1) at room temperature. The components were heated in an oil bath at 80−90 °C for 10 min, mixed by hand at room temperature for 5 min, and reheated in the oil bath at 80−90 °C for 10 min to fully melt the components. The resulting blends were clear and macroscopically homogenous. The liquid crystal was then cooled to room temperature before further use.

Differential Scanning Calorimetry (DSC). Physically, thermochromic behavior occurs due to the Smectic A to twisted nematic phase transition. This mesophase transition was measured by differential scanning calorimetry (Q100, TA Instruments, New Castle, DE). Solid, room-temperature liquid crystal samples (∼4 to 6 mg) were loaded into standard aluminum sample pans using a microspatula. An empty sample pan was used as a reference. Based on previous reports,[31,52] the samples were first annealed by heating to 50 °C at a rate of 20 °C/min and held at 50 °C for 10 min, then cooled to −30 °C at a rate of 20 °C/min. After an isothermal hold at −30 °C for 15 min, the samples were heated to 70 °C, cooled to −30 °C, and heated again to 70 °C at a rate of 10 °C/min. Based on the measured heat flow as a function of temperature (representative thermogram in the Supporting Information, Figure S3), the temperature at which the smectic A to twisted nematic phase transition (LC transition) occurred, as indicated by the endothermic melting peak ∼25 to 30 °C, was determined using TA Instruments Universal Analysis. Samples were run in triplicate. The average LC transition temperature is reported, and the standard deviation is indicated.

Polarized Light Microscopy. While DSC is a practical tool for observing such phase transitions under precise thermal control,[31] we were interested in directly observing the temperature-dependent color under accessible thermal conditions using PLM. To observe thermochromic behavior of the liquid crystal samples, we used rectangular glass capillaries (50 mm × 4 mm × 2 mm $L \times W \times H$) to ensure a flat liquid crystal surface as well as accommodate a thermocouple to monitor the sample temperature. To prepare the sample, the liquid crystals were heated to ∼80 °C to melt the sample. The melted sample was loaded into a 1 mL syringe and then ∼100 μL was transferred to the capillary (22 gauge needle). Both ends of the glass capillaries were sealed with tape and stored at 4 °C before imaging. To monitor the sample temperature, a thermocouple was placed through one end of the capillary into the LC sample (Figure 3). The samples were heated to 45 °C for 2 min with gel hot pads and then the capillary was transferred to the microscope stage. The sample was imaged as it cooled and solidified. The working time before solidification was 1−2 min. To maintain consistent thermal history, the

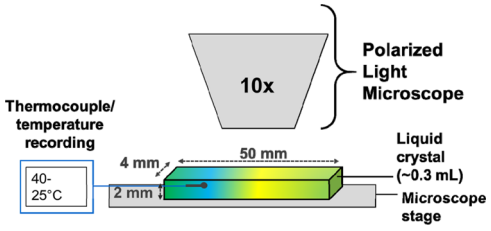

Figure 3. Diagram of the PLM setup for characterizing the thermochromic behavior of liquid crystals. A rectangular (2 mm × 4 mm) glass capillary was filled with the liquid crystal, heated to 45 °C, then placed on the microscope stage; the sample was imaged as it cooled and solidified.

https://dx.doi.org/10.1021/acsomega.9b03484
ACS Omega 2020, 5, 7149−7157

analyzed samples were heated and cooled to room temperature a total of four times prior to analysis.

Samples were imaged using a Nikon Eclipse 150N with cross polarizers (Epi Rotatable Polarizer and L-AN analyzer) at the minimum field diaphragm (i.e., minimum F. stop). At 10× magnification (CFI60-2 TU Plan FLUOR BD Objective Lens), the aperture diaphragm was approximately 50%. The sample was placed on the stage and the illumination (i.e., light intensity) was set to the highest illumination such that the initial frame appeared black to maintain comparable lighting conditions for each sample.

Due to the changes in sample brightness during the color change, videos were recorded using autoexposure and auto white balancing at 1 fps. Without autoexposure, the color change could not be detected due to oversaturation. Due to the use of autoexposure, auto white balancing, a commonly used technique to achieve color constancy between images,[34] was used to capture the perceived color transition from blue to red (representative data comparing a sample recorded with and without autoexposure is shown in the Supporting Information, Figure S1).

We note that videos were recorded with constant illumination and a colorimetrically stable black aperture diaphragm surrounding the thermochromic liquid crystal. In this setup using white balancing with the colorimetrically stable black aperture diaphragm surrounding the thermochromic liquid crystal, the perceived colors of the liquid crystals in the images and the resulting $L^*a^*b^*$ values matched the expected maximum UV−vis reflectance at the corresponding temperature (Figure S2) based on ISO standard 21348. However, we emphasize that the focus of this work is identifying color changes rather than ground truth colors to characterize the thermochromic properties of liquid crystals, i.e., the temperature of the color change events. Specifically, since we use auto white balancing to reproduce our visual observations of the sample, our method analyzes perceived changes between frames.

Video Analysis. From the video that captured the perceived color transition from blue to green to yellow to orange to red, our goal was to develop an objective method to identify the color change events by analyzing differences between each frame as an alternative to manual frame-by-frame analysis. For objective frame-by-frame video analysis, we extracted the individual frames from the video using Python. The RGB color for each pixel in each image was determined; the average RGB values of a 20 × 20 pixel area in the center of the frame were used for analysis. To relate the quantitative analysis with physical observations (namely, the transitions from (1) black to blue, (2) blue to green, (3) green to yellow, (4) yellow to orange, (5) orange to red, and (6) red to black), we transformed the sRGB values to CIE $L^*a^*b^*$ color space, which correlates strongly with human vision. Thus, the conversion to CIE $L^*a^*b^*$ using the inverse γ correction was based on the CIE D_{65} Standard Illuminant and 2° viewing angle similar to previous reports.[2,25] This assumption was tested by verifying that the color changes identified by the video analysis method corresponded to changes in the UV−vis peak reflectance (Table 2).

In CIE $L^*a^*b^*$ color space, color is defined by three axes: L indicating brightness, a-axis indicating a value for red/green, and b-axis indicating a value of blue/yellow. The color difference has been used in many applications (without constant lighting conditions or color calibration) including determining the lycopene content of tomatoes using a smartphone camera,[53] automatically detecting the edges of wounds in images,[54] and identifying minerals from digital images.[35] Additionally, color difference in CIE $L^*a^*b^*$ color space has been to predict if two colors will be noticeably different under different viewing environments.[36] The color difference, ΔE, is the color distance between two colors given by the difference between the L, a^*, b^* values for two colors added in quadrature has been established as a useful measure for identifying color differences between samples observed between cross polarizers.[35]

Therefore, to automate analysis of the video to determine the thermochromic behavior of the liquid crystals, we analyzed each frame relative to the initial frame by using the cumulative color difference relative to the initial frame (L_0, a_0, b_0) (eq 1 below)

$$\begin{aligned}&\text{cumulative color difference}\\ &= E_c\\ &= \sqrt{(L - L_0)^2 + (a - a_0)^2 + (b - b_0)^2}\end{aligned} \quad (1)$$

Examining the cumulative color difference reduces noise compared to simply analyzing the color difference between each frame so that changes in color (i.e., large differences in ΔE) are more readily apparent when performing frame-by-frame analysis. An example of the color cumulative color difference compared to the color difference between each frame is shown in the Supporting Information (Figure S4).

We performed frame-by-frame analysis by comparing the cumulative color difference of each frame, i, to the previous frame, $i - 1$, to determine if there was a change in color from one frame to the next.

$$\Delta E_r = E_{c,i} - E_{c,i-1} > 2.5 \quad (2)$$

Based on previous studies,[36] we empirically determine the ΔE_r that corresponds to a color change event in the video analysis. Initially, we set the threshold for identifying a color change event at a ΔE_r value of 5. This is the ΔE_r that corresponds with a color difference that is perceived by the human eye.[24,55] With a threshold of $\Delta E_r = 5$, fewer than six color change events were observed in our initial method development. Therefore, the threshold was lowered to identify at least six color change events based on the observed color changes. Thus, a color change event was said to occur if the ΔE_r value between consecutive frames was greater than 2.5 (eq 2). This empirically determined threshold is similar to the empirical benchmark previously reported as the "just noticeable" color difference for CIE $L^*a^*b^*$.[36]

Generally, this method identified more than six color change events because there were changes in the sample brightness as it changed in color. Specifically, the samples brightened in the blue region and faded in the red region. Therefore, we next needed to identify the changes in brightness as well as the observed transitions from (1) black to blue, (2) blue to green, (3) green to yellow, (4) yellow to orange, (5) orange to red, and (6) red to black. Based on the physical observations, the first and last identified color changes correspond to the blue-start (black to blue) and red-end (red to black), respectively.

To distinguish between the frame-to-frame color change events identified that were due to changes in brightness and the observed intermediate color transitions, namely, the (2) blue to green, (3) green to yellow, (4) yellow to orange, (5)

https://dx.doi.org/10.1021/acsomega.9b03484
ACS Omega 2020, 5, 7149−7157

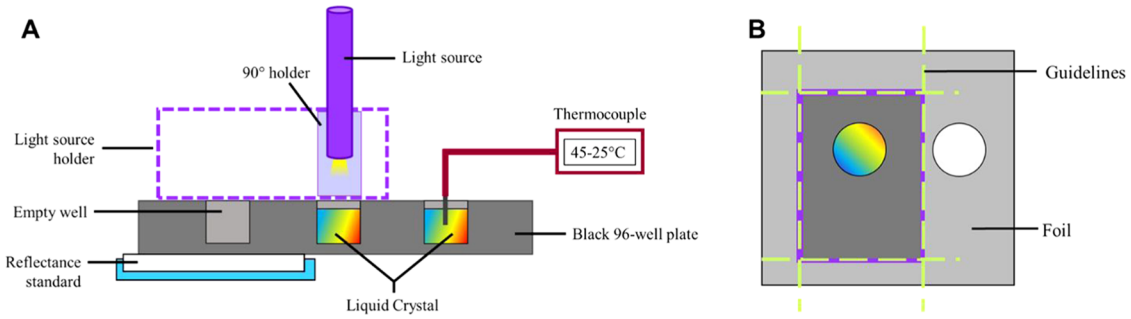

Figure 4. Diagram of the (A) side view and (B) top view of the UV−vis reflectance measurement setup using black 96-well plates covered in foil. The 90° detector holder was used and foil with guidelines was used to minimize light leaking and line up the detector to the well.

orange to red, we calculated the fraction of the frame-to-frame color difference between each frame, i, and the previous frame, $i-1$, that was due to the difference in L, which we defined as $f_{\Delta L}$ (eq 3 below).

$$f_{\Delta L} = \frac{\sqrt{(L_i - L_{i-1})^2}}{\sqrt{(L_i - L_{i-1})^2 + (a_i - a_{i-1})^2 + (b_i - b_{i-1})^2}} \quad (3)$$

This fraction corresponds to the perceived change in brightness compared to the perceived change in color when comparing each frame to the previous frame. Large values of ΔE_r between consecutive frames that were mostly due to changes in brightness (e.g., dark blue to bright blue) would have a relatively large $f_{\Delta L}$. In contrast, large values of ΔE_r between consecutive frames that were due to changes in color (e.g., green to yellow) would have a relatively small value of $f_{\Delta L}$. Thus, the color change events with the four lowest $f_{\Delta L}$ values were said to be the color transitions. Typically, $f_{\Delta L}$ values for color transitions were less than 0.02 compared to changes in brightness with $f_{\Delta L} > 0.2$. The first color transition after the identified blue-start was considered the blue to green transition. The next identified color transitions were considered the green to yellow, yellow to orange, and orange to red transitions.

Based on the video analysis, the thermochromic properties can be described by various parameters, namely, blue-start, red-start, red-end temperatures, bandwidth (temperature difference between the blue-start and red-start temperatures), and color play (temperature difference between blue-start and red-end temperatures) were determined.

UV−Vis Reflectance Measurements. To validate the color changes identified in the video analysis, we used UV−vis reflectance spectroscopy. Specifically, we aimed to verify that the color change events that we identified from the video and the subsequent analysis corresponded with changes in the UV−vis reflectance peak.

UV−vis reflectance spectra (350−1200 nm) of the samples were obtained with an Ocean Optics (Largo, Fl.) Flame spectrometer (FLAME-S-VIS-NIR-ES) was equipped with a tungsten-halogen light source (HL-2000-HP-FHSA, 20 W output) and a reflectance probe (RPH-1) at room temperature using poly(tetrafluoroethylene) (PTFE) as a standard.[56] To acquire reflectance spectra, as the liquid crystal changed color as a function of temperature, the following experimental setup was developed (Figure 4). The liquid crystal sample (0.25 mL) was placed in a 96-well plate with a clear bottom and black sides (Corning, Corning, NY). The plate was covered in foil with only the wells with the liquid crystal and an empty control uncovered. The probe was placed at a 90° position based on the previous work demonstrating that a normal angle improves precision[57] and the PTFE reflectance standard was placed under the empty well as the control (Figure 4A). The liquid crystal was added to a second adjacent well to accommodate a thermocouple to monitor the temperature of the liquid crystal. Guidelines were created on the foil to ensure alignment between the sample and the detector (Figure 4B).

The sample was heated up to ∼45 °C on a hot plate, and spectra were collected every 10 s as the sample cooled to ambient conditions over 10−15 min. In parallel with the spectra, the thermocouple reading was logged every 10 s.

At every time point, wavelengths between 425 and 700 nm were further analyzed. In Excel, the maximum reflectance between 425 and 700 nm was determined and used to normalize the reflectance spectra. The color corresponding to the reflectance spectra was defined using ISO 21348. The position of the leading peak was tracked as a function of time. The blue-start was identified as the first spectra for which the maximum normalized reflectance occurred at a wavelength between 450 and 500 nm. The red-start was identified as the first spectra for which the maximum normalized reflectance occurred between 610 and 760 nm. The red-end was identified as the last spectra for which the maximum normalized reflectance occurred between 610 and 760 nm, occurring consecutively following the red-start. Since there is a decrease in reflectance due to the sample fading (Figure 2), we opt to normalize the reflectance spectra to ease peak detection.

■ ASSOCIATED CONTENT

Supporting Information

The Supporting Information is available free of charge at https://pubs.acs.org/doi/10.1021/acsomega.9b03484.

Polarized light microscopy images recorded with and without autoexposure for comparison; polarized light microscopy images with corresponding $L^*a^*b^*$ values and UV−vis reflected maxima; bandwidth and color play measured by PLM video analysis compared to UV−vis reflectance spectroscopy; a representative DSC thermogram, representative data showing the cumulative color difference compared to color difference between each frame (PDF)

■ AUTHOR INFORMATION

Corresponding Author

Christina Tang − *Chemical and Life Science Engineering, Virginia Commonwealth University, Richmond, Virginia 23284-*

https://dx.doi.org/10.1021/acsomega.9b03484
ACS Omega 2020, 5, 7149−7157

3028, United States; orcid.org/0000-0001-6204-0129; Email: ctang2@vcu.edu

Authors

Shani L. Levit − *Chemical and Life Science Engineering, Virginia Commonwealth University, Richmond, Virginia 23284-3028, United States*

Jimmy Nguyen − *Chemical and Life Science Engineering, Virginia Commonwealth University, Richmond, Virginia 23284-3028, United States*

Nicholas P. Hattrup − *Chemical and Life Science Engineering, Virginia Commonwealth University, Richmond, Virginia 23284-3028, United States*

Briget E. Rabatin − *Chemical and Life Science Engineering, Virginia Commonwealth University, Richmond, Virginia 23284-3028, United States*

Ratib Stwodah − *Chemical and Life Science Engineering, Virginia Commonwealth University, Richmond, Virginia 23284-3028, United States*

Christopher L. Vasey − *Chemical and Life Science Engineering, Virginia Commonwealth University, Richmond, Virginia 23284-3028, United States*

Michael P. Zeevi − *Chemical and Life Science Engineering, Virginia Commonwealth University, Richmond, Virginia 23284-3028, United States*

McKenna Gillard − *Chemical and Life Science Engineering, Virginia Commonwealth University, Richmond, Virginia 23284-3028, United States*

Paola A. D'Angelo − *U.S. Army Combat Capabilities Development Command Soldier Center, Natick, Massachusetts 01760, United States*

Kathleen W. Swana − *U.S. Army Combat Capabilities Development Command Soldier Center, Natick, Massachusetts 01760, United States*

Complete contact information is available at: https://pubs.acs.org/10.1021/acsomega.9b03484

Author Contributions

§S.L.L. and J.N. contributed equally.

Notes

The authors declare no competing financial interest.

■ ACKNOWLEDGMENTS

This work was partially supported by startup funding at Virginia Commonwealth University, Virginia Commonwealth University Presidential Research Quest Fund, NSF (Award No. 1651957), and U.S. Army Combat Capabilities Development Command Soldier Center (Grant No. W911QY-17-2-0003).

■ REFERENCES

(1) van der Werff, L. C.; Robinson, A. J.; Kyratzis, I. L. Combinatorial Approach for the Rapid Determination of Thermochromic Behavior of Binary and Ternary Cholesteric Liquid Crystalline Mixtures. *ACS Comb. Sci.* **2012**, *14*, 605−612.

(2) Sage, I. Thermochromic Liquid Crystals Thermochromic Liquid Crystals. *Liq. Cryst.* **2011**, *38*, 1551−1561.

(3) Pochaczevsky, R.; Wexler, C. E.; Meyers, P. H.; Epstein, J. A.; Marc, J. A. Liquid Crystal Thermography of the Spine and Extremities. *J. Neurosurg.* **1982**, *56*, 386−395.

(4) Ochoa, A. D.; Baughn, J. W.; Byerley, A. R. A New Technique for Dynamic Heat Transfer Measurements and Flow Visualization Using Liquid Crystal Thermography. *Int. J. Heat Fluid FLow* **2005**, *26*, 264−275.

(5) Muwanga, R.; Hassan, I. Local Heat Transfer Measurements in Microchannels Using Liquid Crystal Thermography : Methodology Development and Validation. *J. Heat Transfer* **2006**, *128*, 617−626.

(6) van der Westhuizen, J. E.; Dirker, J.; Meyer, J. P. Implementation of Liquid Crystal Thermography to Determine Wall Temperatures and Heat Transfer Coefficients in a Tube-in-Tube Heat Exchanger. *Exp. Heat Transfer* **2016**, *29*, 632−656.

(7) Stasiek, J.; Jewartowski, M.; Kowalewski, T. A. The Use of Liquid Crystal Thermography in Selected Technical and Medical Applications — Recent Development. *J. Cryst. Process Technol.* **2014**, *4*, 46−59.

(8) Popov, V. M.; Klimenko, A. S.; Pokanevich, A. P.; Gavrilyuk, I. I.; Moshel, N. V. Liquid-Crystal Thermography of Hot Spots on Electronic Components. *Russ. Microelectron.* **2007**, *36*, 392−401.

(9) Ekkad, S. V.; Han, J.-C. A Transient Liquid Crystal Thermography Technique for Gas Turbine Heat Transfer Measurements. *Meas. Sci. Technol.* **2000**, *11*, 957−968.

(10) Armitage, D.; Price, F. P. Calorimetry of Liquid Crystal Phase Transitions. *J. Phys. Colloques* **1975**, *36*, C1-133−C1-136.

(11) Barrall, E. M.; Porter, R. S.; Johnson, J. F. Specific Heats of Nematic, Smectic, and Cholesteric Liquid Crystals by Differential Scanning Calorimetry. *J. Phys. Chem. A* **1967**, *71*, 895−900.

(12) Barall, E. M.; Porter, R. S.; Johnson, J. F. Heat Transition for Some Cholestryl Esters by Differential Scanning Calorimetry. *J. Phys. Chem. B* **1967**, *71*, 1224−1228.

(13) Kılıç, V.; Alankus, G.; Horzum, N.; Mutlu, A. Y.; Bayram, A.; Solmaz, M. E. Single-Image-Referenced Colorimetric Water Quality Detection Using a Smartphone. *ACS Omega* **2018**, *3*, 5531−5536.

(14) Panák, O.; Držková, M.; Kailová, N.; Syrový, T. Colorimetric Analysis of Thermochromic Samples in Different Forms Employing a Digital Camera. *Measurement* **2018**, *127*, 554−564.

(15) Wang, Z.; Ireland, P. T.; Jones, T. V.; Royce, R. A Color Image Processing System for Transient Liquid Crystal Heat Transfer Experiments. *J. Turbomach.* **1996**, *118*, 421−427.

(16) Billmeyer, F. W.; Saltzman, M. *Principles of Color Technology*, 2nd ed.; John Wiley & Sons, 1981.

(17) Solli, M.; Andersson, M.; Lenz, R.; Kruse, B. In *Color Measurements with a Consumer Digital Camera Using Spectral Estimation Techniques*, Scandinavian Conference on Image Analysis, 2005; pp 105−114.

(18) Nyström, D. In *Colorimetric and Multispectral Image Acquisition Using Model-Based and Empirical Device Characterization*, Scandinavian Conference on Image Analysis, 2007; pp 798−807.

(19) Martínez-García, J.; Hébert, M.; Trémeau, A. In *Color Calibration of an RGB Digital Camera for the Microscopic Observation of Highly Specular Materials*, Measuring, Modeling, and Reproducing Material Appearance, 2015; Vol. 9398.

(20) Connah, D.; Westland, S.; Thomson, M. G. A. Recovering Spectral Information Using Digital Camera Systems Coloration Technology. *Color. Technol.* **2001**, *117*, 309−312.

(21) Heikkinen, V.; Lenz, R.; Jetsu, T.; Parkkinen, J.; Hauta-kasari, M.; Jääskeläinen, T. Evaluation and Unification of Some Methods for Estimating Reflectance Spectra from RGB Images. *J. Opt. Soc. Am. A* **2008**, *25*, 2444−2458.

(22) Cherdhirunkorn, K.; Tsumura, N.; Nakaguchi, T.; Miyake, Y. Spectral Based Color Correction Technique Compatible with Standard RGB System. *Opt. Rev.* **2006**, *13*, 138−145.

(23) Tkalčič, M.; Tasič, J. F. In *Colour Spaces-Perceptual, Historical and Applicational Background*, IEEE Reg. 8 EUROCON 2003 Comput. as a Tool-Proceedings, 2003; pp 304−308.

(24) Thornton, B. T. E.; Harrison, A.; Pham, A. L.; Castano, C. E.; Tang, C. Polyaniline-Functionalized Nano Fi Bers for Colorimetric Detection of HCl Vapor. *ACS Omega* **2018**, *3*, 3587−3591.

(25) Yang, R.; Cheng, W.; Chen, X.; Qian, Q.; Zhang, Q.; Pan, Y.; Duan, P.; Miao, P. Color Space Transformation-Based Smartphone Algorithm for Colorimetric Urinalysis. *ACS Omega* **2018**, *3*, 12141−12146.

(26) Jung, Y.; Kim, J.; Awofeso, O.; Kim, H.; Regnier, F.; Bae, E. Smartphone-Based Colorimetric Analysis for Detection of Saliva Alcohol Concentration. *Appl. Opt.* **2015**, *54*, 9183−9189.
(27) Vashist, S. K.; van Oordt, T.; Schneider, E. M.; Zengerle, R.; Stetten, F.; Luong, J. H. T. A Smartphone-Based Colorimetric Reader for Bioanalytical Applications Using the Screen-Based Bottom Illumination Provided by Gadgets. *Biosens. Bioelectron.* **2015**, *67*, 248−255.
(28) Moghaddam, G. K.; Lowe, C. R. Smartphone-Based Quantitative Measurements on Holographic Sensors. *PLoS One* **2017**, *12*, No. e0187467.
(29) Panák, O.; Držková, M.; Kaplanová, M. Insight into the Evaluation of Colour Changes of Leuco Dye Based Thermochromic Systems as a Function of Temperature. *Dyes Pigm. Pigment.* **2015**, *120*, 279−287.
(30) Coleman, B.; Coarsey, C.; Kabir, M. A.; Asghar, W. Point-of-Care Colorimetric Analysis through Smartphone Video. *Sens. Actuators, B* **2019**, *282*, 225−231.
(31) Sharma, D.; Macdonald, J. C.; Iannacchione, G. S. Thermodynamics of Activated Phase Transitions of 8CB : DSC and MC Calorimetry. *J. Phys. Chem. B* **2006**, *110*, 16679−16684.
(32) Frank, S. G.; Byrd, B. G. Phase Transitions in Binary Mixtures of Cholesteryl Esters. *J. Pharm. Sci.* **1972**, *11*, 1762−1765.
(33) Sage, I. Thermochromic Liquid Crystals in Devices. In *Liquid Crystals, Applications and Uses*; Bahadur, B., Ed.; World Scientific: 1990; pp 301−341.
(34) Zhao, Y.; Elliott, C.; Rafferty, K. In *Spectral Illumination Correction: Achieving Relative Color Constancy Under the Spectral Domain*, IEEE International Symposium on Signal Processing and Information Technology, Louisville, KY, 2018; p 5.
(35) Aligholi, S.; Lashkaripour, G. R.; Khajavi, R.; Razmara, M. Automatic Mineral Identification Using Color Tracking. *Pattern Recognit.* **2017**, *65*, 164−174.
(36) Szafir, D. A.; Gleicher, M. L. In *Adapting Color Difference for Design*, Color and Imaging Conference, 2014; pp 228−233.
(37) Bell, G. R. R.; Mäthger, L. M.; Gao, M.; Senft, S. L.; Kuzirian, A. M.; Kattawar, G. W.; Hanlon, R. T. Diffuse White Structural Coloration from Multilayer Reflectors in a Squid. *Adv. Mater.* **2014**, *26*, 4352−4356.
(38) Mcgrath, J. G.; Bock, R. D.; Cathcart, J. M.; Lyon, L. A. Self-Assembly of "Paint-On" Colloidal Crystals Using Poly(Styrene- Co -N -Isopropylacrylamide) Spheres. *Chem. Mater.* **2007**, *19*, 1584−1591.
(39) Makky, M.; Soni, P. In Situ Quality Assessment of Intact Oil Palm Fresh Fruit Bunches Using Rapid Portable Non-Contact and Non-Destructive Approach. *J. Food Eng.* **2014**, *120*, 248−259.
(40) Choudhary, R.; Bowser, T. J.; Weckler, P.; Maness, N. O.; Mcglynn, W. Rapid Estimation of Lycopene Concentration in Watermelon and Tomato Puree by Fiber Optic Visible Reflectance Spectroscopy. *Postharvest Biol. Technol.* **2009**, *52*, 103−109.
(41) Dixon, G. D.; Scala, L. C. Thermal Hysteresis in Cholestic Color Responses. *Mol. Cryst. Liq. Cryst.* **1970**, *10*, 317−325.
(42) Anderson, M. R.; Baughn, J. W. Hysteresis in Liquid Crystal Thermography. *J. Heat Transfer* **2004**, *126*, 339−346.
(43) Zhao, H.; Gao, J.; Pan, Z.; Huang, G.; Xu, X.; Song, Y.; Xue, R.; Hong, W.; Qiu, H. Chemically Responsive Polymer Inverse-Opal Photonic Crystal Films Created by a Self-Assembly Method. *J. Phys. Chem. C* **2016**, *120*, 11938−11946.
(44) Lee, H.-G.; Munir, S.; Park, S.-Y. Cholesteric Liquid Crystal Droplets for Biosensors. *ACS Appl. Mater. Interfaces* **2016**, *8*, 26407−26417.
(45) Liu, L.; Peng, S.; Wen, W.; Sheng, P. Paperlike Thermochromic Display. *Appl. Phys. Lett.* **2007**, *90*, No. 213508.
(46) Wang, J.; Jákli, A.; West, J. L. Airbrush Formation of Liquid Crystal/Polymer Fibers. *ChemPhysChem* **2015**, *16*, 1839−1841.
(47) Ge, D.; Lee, E.; Yang, L.; Cho, Y.; Li, M.; Gianola, D. S.; Yang, S. A Robust Smart Window : Reversibly Switching from High Transparency to Angle-Independent Structural Color Display. *Adv. Mater.* **2015**, *27*, 2489−2495.
(48) Wang, J.; Jákli, A.; Guan, Y.; Fu, S.; West, J. Developing Liquid-Crystal Functionalized Fabrics for Wearable Sensors. *Inf. Disp.* **2017**, *33*, 16−20.
(49) Jasek, K.; Pasternak, M.; Ganicz, T.; Sta, W. A. Liquid Crystal Coating for SAW Sensors. *Eur. Phys. J.: Spec. Top.* **2008**, *154*, 103−106.
(50) Lee, S. S.; Seo, H. J.; Kim, Y. H.; Kim, S.-H. Structural Color Palettes of Core − Shell Photonic Ink Capsules Containing Cholesteric Liquid Crystals. *Adv. Mater.* **2017**, *29*, No. 1606894.
(51) Fujisawa, N.; Aoyama, A.; Kosaka, S. Measurement of Shear-Stress Distribution over a Surface by Liquid-Crystal Coating. *Meas. Sci. Technol.* **2003**, *14*, 1655−1661.
(52) Shanks, R. A.; Staszczyk, D. Thermal and Optical Characterization of Polymer-Dispersed Liquid Crystals. *Int. J. Polym. Sci.* **2012**, *2012*, No. 767581.
(53) Ye, X.; Izawa, T.; Zhang, S. Rapid Determination of Lycopene Content and Fruit Grading in Tomatoes Using a Smart Device Camera. *Cogent Eng.* **2018**, *5*, 1−15.
(54) Papazoglou, E. S.; Zubkov, L.; Mao, X.; Neidrauer, M.; Rannou, N.; Weingarten, M. S. Image Analysis of Chronic Wounds for Determining the Surface Area. *Wound Repair Regen.* **2010**, *18*, 349−358.
(55) Huang, Y.; Chen, M.; Ouhyoung, M. In *Perceptual-Based CNN Model for Watercolor Mixing Prediction*, ACM SIGGRAPH 2018 Posters, 2018; pp 1−2.
(56) Binitha, N. N.; Sugunan, S. Polyaniline/Pillared Montmorillonite Clay Composite Nanofibers. *J. Appl. Polym. Sci.* **2008**, *107*, 3367−3372.
(57) Badiane, A.; Perez i de Lanuza, G.; Garcia-Custodio, M. D.; Carazo, P.; Font, E. Colour Patch Size and Measurement Error Using Reflectance Spectrophotometry. *Methods Ecol. Evol.* **2017**, *8*, 1585−1593.

https://dx.doi.org/10.1021/acsomega.9b03484
ACS Omega 2020, 5, 7149−7157